International Symposium
On Turbulence and Shear Flow
Phenomena (TSFP-8)
August 28 - 30, 2013 Poitiers, France

MULTI-PHASE BLOOD FLOW MODELLING IN AN INTRACRANIAL ANEURYSM CONSIDERING POSSIBLE TRANSITION TO TURBULENCE

Philipp Berg
Lab. of Fluid Dynamics & Technical Flows
University of Magdeburg "Otto von Guericke"
Universitaetsplatz 2, 39106 Magdeburg, Germany
Philipp.Berg@ovgu.de

Abouelmagd Abdelsamie
Lab. of Fluid Dynamics & Technical Flows
University of Magdeburg "Otto von Guericke"
Universitaetsplatz 2, 39106 Magdeburg, Germany
Abouelmagd.Abdelsamie@ovgu.de

Gábor Janiga
Lab. of Fluid Dynamics & Technical Flows
University of Magdeburg "Otto von Guericke"
Universitaetsplatz 2, 39106 Magdeburg, Germany
Gabor.Janiga@ovgu.de

Dominique Thévenin
Lab. of Fluid Dynamics & Technical Flows
University of Magdeburg "Otto von Guericke"
Universitaetsplatz 2, 39106 Magdeburg, Germany
Dominique.Thevenin@ovgu.de

ABSTRACT

Intracranial aneurysms are abnormal dilatations of the cerebral arteries that are, in case of a rupture, highly life-threatening. Numerical investigations carried out to support clinical physicians are commonly assuming laminar flow conditions. However, especially in diseased arteries transition to turbulence has been observed.

To identify a possible transition, the effect of geometry as well as of blood cells were investigated in the present work. Therefore, hemodynamic simulations were carried out under realistic flow conditions in an idealized basilar tip aneurysm. In addition, the impact of blood cells is examined using DNS with a pseudo-spectral code, adding Lagrangian spherical particles (using a point force approach) mimicking the suspension.

The statistical analyses revealed that even under normal flow conditions fluctuations are observed during the cardiac cycle. These appear at relatively high frequencies, around 100 Hz. Additionally, the particulate phase significantly influenced the flow stability.

Hence, the results indicate that transitional effects might indeed play a role to understand hemodynamics and rupture of intracranial aneurysms, and should be accordingly taken into account.

INTRODUCTION

According to the Dorland Medical Dictionary a cerebral aneurysm is an abnormal bulge or ballooning in a blood vessel supplying the brain. Intracranial aneurysms can rupture and bleed into the area between the brain and the surrounding membrane. A noticeable percentage of the human population, typically 2 to 5% depending on the country, harbors a cerebral aneurysm, but only about 0.1% of those aneurysms rupture annually (Kaminogo et al., 2003).

However, the rupture of a cerebral aneurysm leads in up to 90% of all cases to a subarachnoid hemorrhage (SAH). More than 50% of the patients affected by SAH die within the first 6 months. These facts emphasize the importance of a careful investigation of the blood flows in cerebral aneurysms in order to understand and prevent rupture using appropriate treatments (Seshadhri et al., 2011; Janiga et al., 2012).

In order to obtain accurate three-dimensional and time-dependent flow information in cerebral aneurysms, an enormous computational effort is required. Hence, several simplifications are usually employed to decrease model complexity and therefore the computational costs. The non-Newtonian behavior of blood is often neglected since shear-thinning effects first appear at small vessel diameters (Cebral et al., 2005). Almost systematically, blood flow is assumed to be laminar with constant flow properties, which is up to now commonly accepted for intracranial vessels. However, a few groups have recently shown the existence of fluctuating flow structures within the human vascular system (Antiga and Steinman, 2009; Valen-Sendstad et al., 2011), which could be interpreted as a transition to turbulence followed by relaminarization after peak systole. These fluctuations were found in idealized as well as in patient-specific intracranial aneurysms (Ford and Piomelli, 2012).

Non-laminar flow behaviour was observed especially in the case of diseased arteries (e.g., caused by a stenosis) or around strong bifurcations, although diameter-based Reynolds numbers $Re < 500$ were calculated (Khanafer et al., 2007; Lee et al., 2008). Transitional effects occurring around peak systole might have a significant impact on the weakened vessel layers and should be further investigated as a possible explanation for rupture.

In order to save computational costs, it is also commonly accepted to treat blood as a pure liquid. But it is indeed a thick suspension. Blood contains several cellular components that may influence the flow behaviour and hence have a significant impact on the flow stability. The stability of laminar particle-laden flows has been investigated in many works, for instance in the seminal paper by

Saffman (1961). This paper considered a plane parallel flow with two different particle configurations: very fine particles and coarse particles. Using the Orr-Sommerfeld equation he concluded that the fine dust destabilizes the gas whereas the coarse dust stabilizes the continuous flow. Similar results have been found for mixing layer using DNS and the Orr-Sommerfeld equation by Tong & Wang (1998). In spite of numerous studies, many issues are still poorly understood in such two-phase flows, in particular concerning transition and relaminarization. For instance, Klinkenberg *et al.* (2011) and Klinkenberg *et al.* (2013) recently examined the stability and transition for particle-laden channel flows.

To investigate transition or stability, high-resolution techniques are necessary. For a computational study, this means relying on Direct Numerical Simulation (DNS). DNS requires high accuracy solvers. In the present case, a pseudospectral technique is employed.

The hemodynamic flow in intracranial aneurysms involves different typical features: strong time-dependent variations, large-scale vortical structures, shear flow, jet impacting the wall, additionally with a possible impact of the cell loading. A transition to turbulence can in principle happen due to two reasons: due to the geometry of the aneurysm in connection with a time-dependent boundary condition, or due to the impact of the blood cells (two-phase effect). Of course, a combination of both is also possible. In the current paper we try to obtain a clear picture about how each of them contributes to a possible transition and relaminarization. Therefore, laminar but time-dependent simulations are carried out at high resolution in an idealized basilar tip aneurysm, considering blood as a pure liquid. Analyzing the resulting inflow jet into the aneurysm sac, a stability analysis becomes possible. Regarding now the impact of blood cells, possible instabilities are examined that might be caused by the particulate phase. For this purpose, DNS is carried out with point force Lagrangian spherical particles as a first model for the blood cells, investigating modifications of the turbulent features. Combining both studies, the validity of the classical assumption (laminar flow conditions) can be checked.

METHODS

In this section, the employed numerical/computational techniques and configurations will be discussed.

Vascular Geometry and Spatial Discretization

Since the present study was first motivated by the work of Ford and Piomelli (2012), a similar computational domain was reproduced as in their publication. The surface of an idealized basilar tip aneurysm was generated using the CAD software Solid Edge V. 18 (Siemens PLM Software, Plano, Texas, USA). It contains one feeding and two outflow pipes, respectively, which represent the basilar artery as well as the left and right posterior cerebral artery. The corresponding geometric parameters are based on the inlet diameter (D), which was chosen to be 2.6 mm. In order to satisfy Murray's law that describes the physiological principle of minimum work, both outlets have a diameter of $0.8D$. The aneurysm itself possesses a diameter of $9D$. Finally, all three vessels are $14D$ in length. Figure 1 shows the model from three directions as well as an isometric perspective.

The generated aneurysm model was spatially discretized using tetrahedral and prismatic elements. ANSYS ICEM-CFD 14.0 (Ansys Inc., Canonsburg, PA, USA) served as meshing software. Thereby, three stages of refinement were chosen, classified as coarse, intermediate and fine. The corresponding meshes contained approximately 109 000, 589 000 and 1.9 million elements, respectively. Local refinement was applied in regions of high curvature, e.g. the aneurysm neck, and especially in the transition between the feeding artery and the bulb. In order to resolve the velocity gradients close to the arterial wall, up to four prism layers were inserted. Their initial height ranged from 97 to 33 μm and a growth ratio of 1.2 was defined. A previous study of Berg et al. (2012) showed that mesh-independent solutions are achieved at this level of refinement.

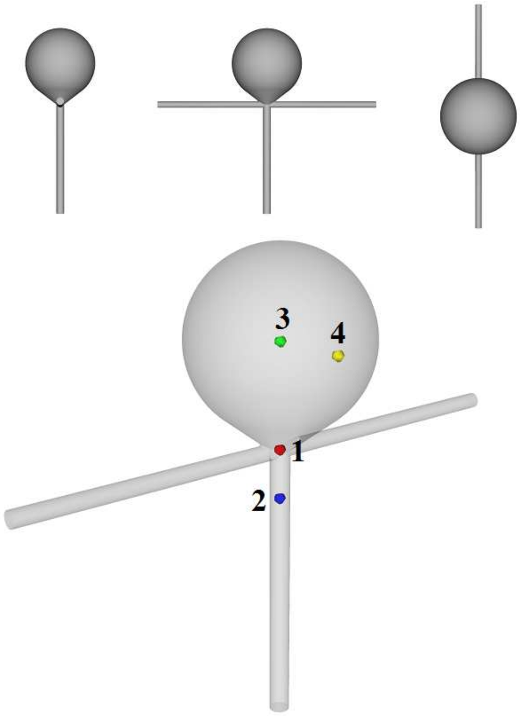

Figure 1. Representation of the idealized basilar tip aneurysm visualized from four perspectives. The spheres indicate the probes used for later statistical analyses: probe 1 (red), probe 2 (blue), probe 3 (green), probe 4 (yellow).

Single-Phase Blood Flow

The generated meshes were used to carry out several hemodynamic simulations with the open-source software package OpenFOAM 2.1.x (ESI Group, Paris, France). To solve the integral formulation of the governing Navier-Stokes equations for continuity and momentum conservation, the unsteady solver pimpleFoam was chosen.

Here, blood is simply treated as an isothermal, incompressible ($\rho = 1050$ kg/m^3) and Newtonian fluid with a constant dynamic viscosity $\eta = 4.265 \cdot 10^{-3}$ Pa·s. Although the viscosity of blood can show a clear shear dependency, a comparison with the typically used Carreau-Yasuda model showed no significant difference in the velocity profiles for the present range of vessel diameters.

In contrast to analytically described inflow conditions, which are based on numerous assumptions, flow rates extracted from 7-Tesla MRI measurements of a healthy volunteer were implemented at the inlet of the basilar artery. The time-dependent values were extracted from the raw image data using EnSight 9.2 (CEI, Apex, NC, USA) and a post-processing tool developed by Stalder *et al.* (2008). All arterial walls were assumed to be rigid and no-slip boundary conditions have been applied. In contrast to significant vessel wall motions in the aortic arch, the radial dilatation of intracranial arteries does not increase more than 5% of the diameter (Valencia et al., 2008). Since it is at present impossible to measure patient-specific wall properties, fluid-structure interaction processes cannot be accounted for. The only possibility would be to assume homogeneous and isotropic material properties as well as a constant wall thickness, which is completely unrealistic. Accurate wall and wall properties information must become measurable before such aspects are taken into account in future simulations.

For both outlets a constant pressure value was defined, assuring an equal outflow. This standard approach was chosen due to the lack of knowledge regarding the pressure variation in the different vessel branches.

The cardiac cycle had a length of $T = 0.85$ s. A constant time step size was chosen as $4.25 \cdot 10^{-5}$ s, according to the stability condition (Courant number < 1), which was estimated in advance. Therefore, each simulation contained 20 000 time steps, which were discretized by a second-order implicit Crank-Nicholson scheme. Convergence was obtained when the scaled residuals of pressure and momentum decreased below a value of 10^{-4} within each time step. Due to the high number of elements the computational domains have been decomposed in advance in order to simulate in parallel using 8 CPUs (AMD Quad Core 2.1 GHz).

Since the Reynolds numbers of the measured flow rates were in the range of 189-254 and since previous works detected fluctuations at Re around 500 (e.g. Ford and Piomelli (2012)), the implemented flow rates were doubled in a second simulation in order to test the effect of a higher inflow. Finally, six unsteady simulations (two different flow rates, three different grids) were carried out without any turbulence model.

The statistical analyses were performed in the third cardiac cycle, discarding the first two in order to reach periodic solutions. The post-processing for the laminar simulations contained cut plane visualizations of the velocity as well as data analysis at four different probes (shown in Fig. 1). These were chosen to be located close to the neck of the aneurysm, before the bifurcation, directly within the bulb as well as close to the aneurysm wall (outside of the inflow jet). For spectral analyses, 20000 time steps have been considered at each probe.

Mathematical Description of the Particulate Flow

Many previous studies have revealed that small solid spherical particles enhance the turbulence intensity (Ferrante and Elghobashi, 2003; Abdelsamie and Lee, 2012; Abdelsamie and Lee, 2013). Additionally, it is known that fine dust may destabilize a laminar flow (Saffman, 1961).

In the present study, a Eulerian-Lagrangian approach is used to compute the coupled dynamics of fluid and particulate phase by DNS. As a first, crude representation of blood cells, solid spherical particles are considered whose diameter, d, is smaller than the smallest flow length scale (as defined in the next section). These particles are released in an incompressible, isotropic flow. The governing equations for the carrier-phase are the Navier-Stokes equations, i.e.

$$\frac{\partial u_i}{\partial t} = -\frac{\partial}{\partial x_i}\left(\frac{p}{\rho} + \frac{u_j u_j}{2}\right) + \epsilon_{ijk} u_j \omega_k + \nu \frac{\partial^2 u_i}{\partial x_j \partial x_j} + f_i\,, \tag{1}$$

and the incompressible fluid continuity equation,

$$\frac{\partial u_i}{\partial x_i} = 0\,, \tag{2}$$

where the alternating tensor ϵ_{ijk} represents the cross product between the fluid velocity u and vorticity ω. In Eq.(1) p is the fluid pressure, ρ and ν are the fluid density and kinematic viscosity, respectively. Furthermore, f_i is the force per unit mass due to the two-way coupling which is opposite of that applied to the particles by the fluid such that:

$$f_i = -\frac{1}{\rho_f}\sum_{n=1}^{N_p} f_i^n(\vec{x}_p^n)\,\delta(\vec{x} - \vec{x}_p^n), \tag{3}$$

where $\delta(\vec{x})$ is a three dimensional Dirac delta function, N_p is the number of dispersed particles in a unit volume of the fluid, and f_i^n is the force exerted on the particle calculated from the particle's equation of motion as follows:

$$\begin{aligned} f_i^n(\vec{x}_p^n) &= m_p\left(\frac{\mathrm{dv}_i^n}{dt}\right) \\ &= \frac{m_p\,(\tilde{u}_i^n - \mathrm{v}_i^n)}{\tau_p}, \end{aligned} \tag{4}$$

$$\frac{dx_{p,i}^n}{dt} = \mathrm{v}_i^n. \tag{5}$$

Here, v, m_p and $x_{p,i}$ are the particulate phase velocity, mass and i-th component of its position vector.

Numerics for DNS of Particulate Flow

In order to scale the current problem, we have retained the smallest time scale as $\tau_k = (\nu/\varepsilon)^{1/2}$ and the smallest length scale as $l_k = (\nu^3/\varepsilon)^{1/4}$. For homogeneous isotropic turbulence those scales would properly degenerate back to the standard Kolmogorov scales, where ε is the dissipation rate of the flow kinetic energy:

$$\varepsilon = 2\nu < S_{ij} S_{ij} >, \tag{6}$$

$$S_{ij} = (\partial u_i/\partial x_j + \partial u_j/\partial x_i)/2. \tag{7}$$

Before introducing the particles, a quasi-laminar initial flow field was obtained starting from a well-prescribed turbulence, after letting it decay from a Taylor Reynolds number $\mathrm{R}_\lambda = 42$ (initial value) to $\mathrm{R}_\lambda = 3$ (just before introducing the particles). The main purpose of this approach is to keep suitable reference scales and start from a flow field

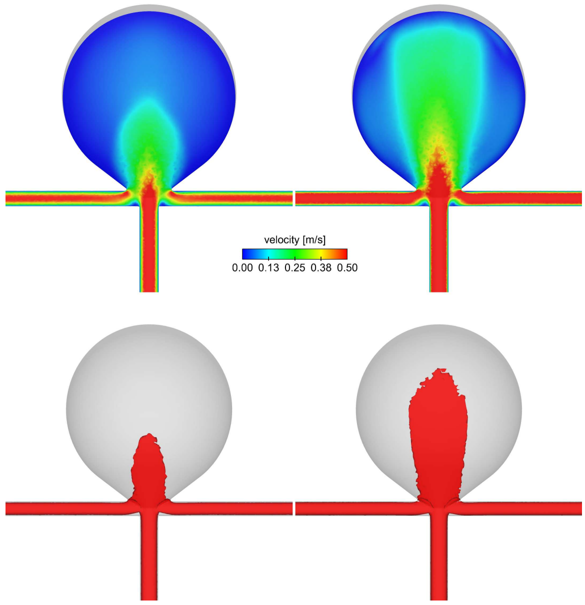

Figure 2. Peak-systolic velocity magnitude and iso-surface (0.2 m/s) shown for the highest mesh resolution: patient-specific flow rate (left), doubled flow rate (right).

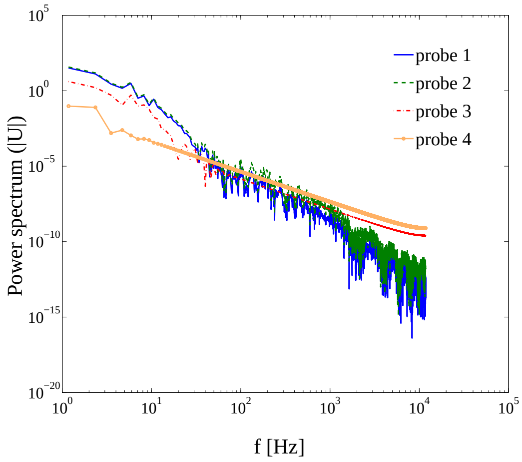

Figure 3. Power spectrum for velocity corresponding to the case with measured flow rates.

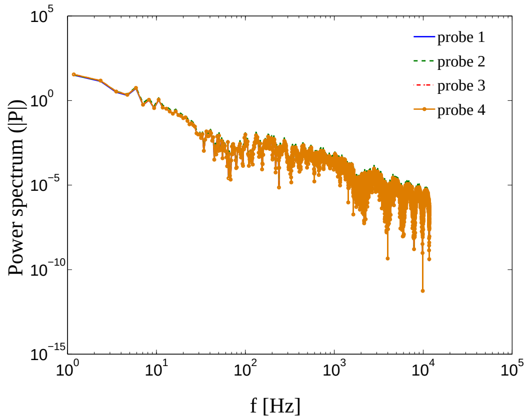

Figure 4. Power spectrum for pressure corresponding to the case with measured flow rates.

with well-defined and statistically reproducible properties. As needed for DNS, all physical scales are resolved during the simulation. Using the pseudospectral solver described in detail in Abdelsamie and Lee (2012), 64^3 regular grid points are placed in a periodic cubic domain. The numerical representation of the particles in the DNS relies on the point force approach. In this approach the variables were interpolated from Eulerian space to Lagrangian space using 4th order Hermite interpolation, whereas they were interpolated back from Lagrangian to Eulerian using a 3-point approximation of the Dirac delta function.

RESULTS AND DISCUSSION

In order to evaluate the impact of the geometry and of the resulting flow structures, cut planes were positioned at one symmetry plane of the aneurysm model. In all cases it was noticed that a symmetrical inflow occurred, directed towards the dome of the aneurysm. This behaviour is expected for laminar flow conditions. Due to the widening of the geometry the velocity magnitude decreases rapidly and shows relatively small values in areas close to the aneurysm wall (Fig. 2), as cleary shown by corresponding iso-surfaces. A threshold of 0.2 m/s was chosen to indicate the regions where higher velocities change to slower ones. Results with the finest grid resolution are shown in Fig. 2 for the really measured as well as for the artificially doubled Reynolds numbers. Regarding mesh density, significant fluctuations in pressure and velocity were present only when using the finest mesh, with almost no effect for the coarse and intermediate ones (not presented here in the interest of space). Therefore, further statistical analyses were carried out only for the finest resolution. This is again a proof that a very high resolution in space and time is indeed needed to capture the true physics of the process.

The spectral analysis of the time-dependent velocity as well as the pressure revealed different phenomena at the different probes. High oscillations at frequencies larger than 40 Hz can be observed especially in probe 1 and 2 (see Figs. 3 and 4). Probe 3 shows a similar behaviour but at frequencies in a range from 20 to 90 Hz, while at higher values the power spectrum decreases monotonically. This effect can be seen for probe 4 as well, which is located close to the aneurysm wall and experiences nearly no fluctuation at all. Therefore, a laminar flow could be assumed in this region. However, fluctuations can be observed at high frequencies at all probes in the pressure power spectrum (Fig. 4).

Combining these observations, the simulations indicate that oscillations are particularly strong within and near the jet of the feeding artery. High fluctuations are seen at the neck of the aneurysm that decrease in areas close to the aneurysm wall. Therefore, the inflow jet seems to show some instability that might be associated with transitional effects. Overall, these findings are in a good agreement with those of Ford and Piomelli (2012).

However, we repeated the simulations in a straight pipe (same diameter, 30 D in length) with a time-dependent inflow condition corresponding to Reynolds numbers ranging from 120 to 250. The corresponding FFT analyses resulted in similar fluctuations of the power spectra at the inlet itself as well as for several probes within the pipe domain. In contrast, constant spectra (no fluctuations) were achieved for steady conditions at the inflow. This may suggest that the observed oscillations are mainly caused by the unsteadiness

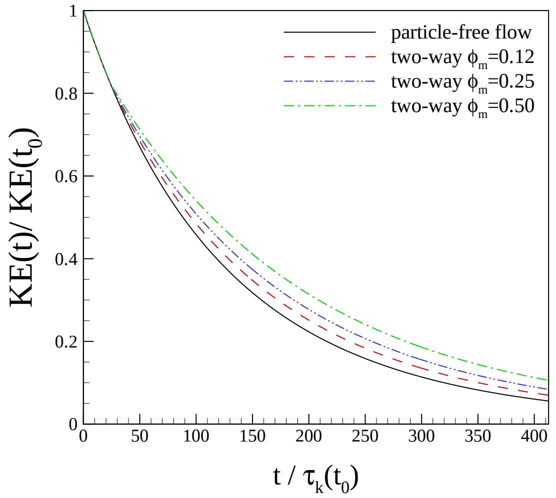

Figure 5. Flow kinetic energy.

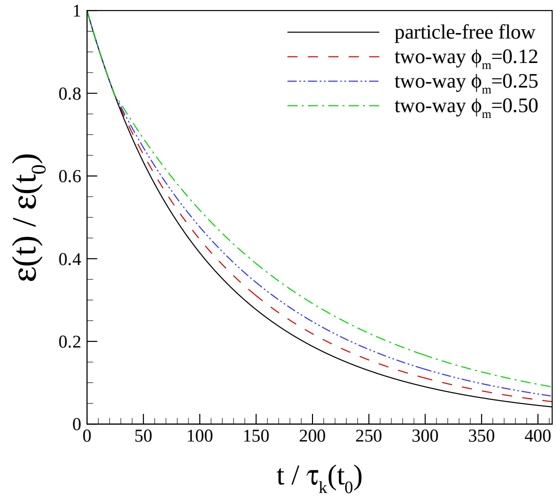

Figure 6. Flow kinetic energy dissipation rate.

of the boundary condition implemented in OpenFOAM and are not only a result of transitional effects. Further studies will be needed to clarify this issue.

In the second part of this section the impact of particles mimicking blood cells is investigated. The statistics of four different cases are examined in this section, based on particle mass fraction/loading in the flow (ϕ_m = 0%, 12%, 25% and 50%), where ϕ_m =0% means a particle-free flow (pure liquid). Stokes number based on the smallest time scale, St= τ_p/τ_k, is in the order of 0.05 (τ_p is the particle relaxation time). Since 99% of the cellular components in blood are red blood cells, the haematocrit and therefore the solid phase consists mainly of erythrocytes. In healthy persons, haematocrit values can be found in a range between 40 to 50%. Therefore, the highest mass load used in DNS represents a realistic situation.

Figures 5 and 6 show temporal flow kinetic energy ($k = 0.5\langle u_i^2\rangle$) and its dissipation rate, ε, respectively (t_0 represents initial time and $\langle\cdot\rangle$ represents the spatial average). They reveal that the flow kinetic energy enhances monotonically with mass loading (Fig. 5). In other words, the decaying rate of the kinetic energy reduces monotonically with increasing particle mass loading. At the same time, the dissipation rate of the kinetic energy enhances monotonically with mass loading (Fig. 6).

A plausible physical interpretation for the previous observations is as follows. Since the presence of particles enhances the flow kinetic energy, the particles work as kinetic energy source. Due to their inertia, they do not lose the energy which they earned from the flow as fast as the flow itself (note that the particles are initially injected with the local flow velocity). Therefore, the particles add additional energy to the flow, which will cause a reduction in the decaying rate. This additional energy should be dissipated due to viscosity effects, which increases the dissipation rate at the flow small length scale (l_k) and time scale (τ_k), as it can be seen from Figs. 7 and 8, respectively.

Using the definitions given in the previous section, the small scales of the flow depend on the kinetic energy dissipation rate. Therefore, the smallest flow length and time scales decrease monotonically with mass loading (Figs. 7 and 8). These observations all document a destabilization of the flow associated to mass loading. Adding more and more particles, the flow shows turbulent features longer and

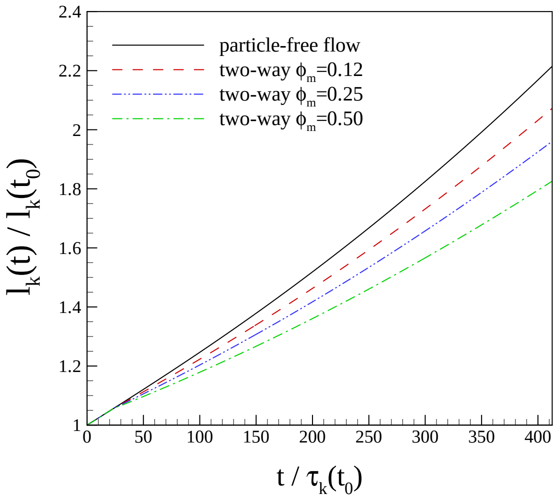

Figure 7. Flow smallest length scale.

stronger than for the same flow without particle loading. Consequently, considering the effect of the blood cells in hemodynamics might be important to understand transition and relaminarization in cerebral flows.

CONCLUSION

The investigation of the impact of a basilar tip aneurysm on the intracranial hemodynamics indicates that non-laminar effects are present, at least when a clear inflow jet into the aneurysmal sac is observed. Strong fluctuations in the power spectra indicate flow oscillations that might have an impact on rupture prediction. Therefore, a suitable resolution in space and time is absolutely necessary to capture the full physics. Since not all cerebral aneurysms are located at bifurcations, high frequency oscillations might not always exist. Further cases need to be evaluated in order to clarify whether the current findings hold in general or not or if the fluctuations in the spectra are mainly caused by the unsteadiness of the implemented boundary condition.

Using DNS it was observed that the particulate phase has a significant influence on flow transition and relaminarization. Therefore, any investigation pertaining to turbulent

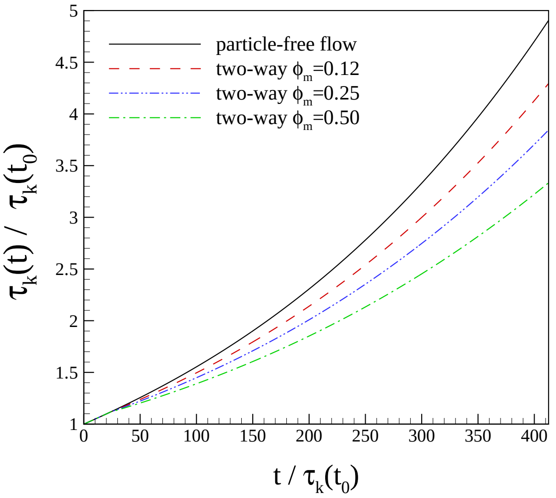

Figure 8. Flow smallest time scale.

fluctuations in cerebral flows should consider the two-way coupling between the flow and the particulate phase. First results show that the particles reduce and delay relaminarization. The impact of non-spherical and, ultimately, deformable particles will be considered in the future.

ACKNOWLEDGEMENT

The authors like to express their gratitude to the International Max Planck Research School for Analysis, Design and Optimization in Chemical and Biomedical Process Engineering Magdeburg for financial support. We would also like to acknowledge Dr. Róbert Bordás for his assistance regarding the FFT analyses.

REFERENCES

Abdelsamie, A. H. & Lee, C. 2012 Decaying versus stationary turbulence in particle-laden isotropic turbulence: Turbulence modulation mechanism. *Physics of Fluids* **24**, 015106.

Abdelsamie, A. H. & Lee, C. 2013 Decaying versus stationary turbulence in particle-laden isotropic turbulence: Heavy particle statistics modifications. *Physics of Fluids* **25**, 033303.

Antiga, L. & Steinman, D. A. 2009 Rethinking turbulence in blood. *Biorheology* **46** (2), 77–81.

Berg, P., Janiga, G. & Thévenin, D. 2012 Detailed comparison of numerical flow predictions in cerebral aneurysms using different CFD software. In *Conference on Modelling Fluid Flow* (ed. J. Vad), vol. **15**, pp. 128–135.

Cebral, J. R., Castro, M. A., Appanaboyina, S., Putman, C. M., Millan, D. & Frangi, A.F. 2005 Efficient pipeline for image-based patient-specific analysis of cerebral aneurysm hemodynamics: technique and sensitivity. *IEEE Transactions on Medical Imaging* **24** (4), 457–467.

Ferrante, A. & Elghobashi, S. 2003 On the physical mechanisms of two-way coupling in particle laden isotropic turbulence. *Physics of Fluids* **15**, 318–329.

Ford, M. D. & Piomelli, U. 2012 Exploring high frequency temporal fluctuations in the terminal aneurysm of the basilar bifurcation. *Journal of Biomechanical Engineering* **134 (9)**, 091003.

Janiga, G., Rössl, C., Skalej, M. & Thévenin, D. 2012 Realistic virtual intracranial stenting and computational fluid dynamics for treatment analysis. *Journal of Biomechanics* **46**, 7–12.

Kaminogo, M., Yonekura, M. & Shibata, S. 2003 Incidence and outcome of multiple intracranial aneurysms in a defined population. *Stroke* **34** (1), 16–21.

Khanafer, K.M., Bull, J.L., Upchurch, G.R. & Berguer, R. 2007 Turbulence significantly increases pressure and fluid shear stress in an aortic aneurysm model under resting and exercise flow conditions. *Annals of Vascular Surgery* **21** (16), 67–74.

Klinkenberg, J., Lange, H. C. de & Brandt, L. 2011 Modal and non-modal stability of particle-laden channel flow. *Physics of Fluids* **23**, 064110.

Klinkenberg, J., Sardina, G., Lange, H. C. de & Brandt, L. 2013 Numerical study of laminar-turbulent transition in particle-laden channel flow. *Physical Review E*, accepted for publication.

Lee, S. E., Lee, S. W., Fischer, P.F., Bassiouny, H.S. & Loth, F. 2008 Direct numerical simulation of transitional flow in a stenosed carotid bifurcation. *Journal of Biomechanics* **41** (16), 2551–2561.

Saffman, P. G. 1961 Fluid-to-fluid conjugate heat transfer for a vertical pipe - internal forced convection and external natural convection. *Journal of Fluid Mechanics* **13**, 120–128.

Seshadhri, S., Janiga, G., Beuing, O., Skalej, M. & Thévenin, D. 2011 Impact of stents and flow diverters on hemodynamics in idealized aneurysm models. *Journal of Biomechanical Engineering* **133** (7), 071005.

Stalder, A. F., Russe, M. F., Frydrychowicz, A., Bock, J., Hennig, J. & Markl, M. 2008 Quantitative 2D and 3D phase contrast MRI: Optimized analysis of blood flow and vessel wall parameters. *Society of Magnetic Resonance in Medicine* **60**, 1218–1231.

Tong, X.-L. & Wang, L.-P. 1998 Two-way coupled particle-laden mixing layer. part 1: Linear instability. *International Journal of Multiphase Flow* **25**, 575–598.

Valen-Sendstad, K., Mardal, K. A., Mortensen, M., Reif, B.A.P. & Langtangen, H.P. 2011 Direct numerical simulation of transitional flow in a patient-specific intracranial aneurysm. *Journal of Biomechanics* **44** (16), 2826–2832.

Valencia, A., Ledermann, D., Rivera, R., Bravo, E. & Galvez, M. 2008 Blood flow dynamics and fluid-structure interaction in patient-specific bifurcating cerebral aneurysms. *International Journal for Numerical Methods in Fluids* **58** (10), 1081–1100.